UC Riverside
UC Riverside Previously Published Works

Title

Micellar and structural stability of nanoscale amphiphilic polymers: Implications for anti-atherosclerotic bioactivity

Permalink

https://escholarship.org/uc/item/7z64582z

Authors

Zhang, Yingyue
Li, Qi
Welsh, William J
et al.

Publication Date

2016-04-01

DOI

10.1016/j.biomaterials.2015.12.028

Peer reviewed

Micellar and Structural Stability of Nanoscale Amphiphilic Polymers: Implications for Anti-atherosclerotic Bioactivity

Yingyue Zhang[1], **Qi Li**[2], **William J. Welsh**[3], **Prabhas V. Moghe**[2], and **Kathryn E. Uhrich**[1,2,*]

[1]Department of Chemistry and Chemical Biology, Rutgers University, Piscataway, NJ 08854, USA

[2]Department of Biomedical Engineering, Rutgers University, Piscataway, NJ 08854, USA

[3]Department of Pharmacology, Robert Wood Johnson Medical School, Rutgers University, New Brunswick 08901, USA

Abstract

Atherosclerosis, a leading cause of mortality in developed countries, is characterized by the buildup of oxidized low-density lipoprotein (oxLDL) within the vascular intima, unregulated oxLDL uptake by macrophages, and ensuing formation of arterial plaque. Amphiphilic polymers (AMPs) comprised of a branched hydrophobic domain and a hydrophilic poly(ethylene glycol) (PEG) tail have shown promising anti-atherogenic effects through direct inhibition of oxLDL uptake by macrophages. In this study, five AMPs with controlled variations were evaluated for their micellar and structural stability in the presence of serum and lipase, respectively, to develop underlying structure-atheroprotective activity relations. In parallel, molecular dynamics simulations were performed to explore the AMP conformational preferences within an aqueous environment. Notably, AMPs with ether linkages between the hydrophobic arms and sugar backbones demonstrated enhanced degradation stability and storage stability, and also elicited enhanced anti-atherogenic bioactivity. Additionally, AMPs with increased hydrophobicity elicited increased atheroprotective bioactivity in the presence of serum. These studies provide key insights for designing more serum-stable polymeric micelles as prospective cardiovascular nanotherapies.

Keywords

Amphiphilic polymers; atherosclerosis; micelle; serum stability; structure-activity relationship

1. INTRODUCTION

The American Heart Association's 2015 statistics cite cardiovascular disease (CVD) to be the leading cause of death globally, accounting for 17.3 million deaths per year. By 2030,

*Corresponding author, Department of Chemistry and Chemical Biology, Rutgers University, 610 Taylor Road, Piscataway, New Jersey 08854, USA, Telephone number: (848) 445-0361, Fax number: (732) 445-7036, keuhrich@rci.rutgers.edu.

the mortality number is expected to grow to more than 23.6 million [1]. Atherosclerosis is an inflammatory disease characterized by increased plasma levels of low-density lipoprotein (LDL), which ultimately lead to arterial plaque development, a key pathology underlying CVDs. During the early stages of the disease, LDL circulating in the bloodstream infiltrates into the injured arterial wall and accumulates in the subendothelial space, where it undergoes oxidative modification to oxidized LDL (oxLDL). OxLDL triggers monocyte recruitment and their differentiation into macrophages, which leads to scavenger receptor (SR) upregulation on cell surfaces. In addition, the reduced localized positive charge of oxLDL leads to the reduced recognition by the classical LDL receptors but increased affinity to SRs on macrophages [2]. While the uptake of native LDL via LDL receptor is regulated by the intracellular cholesterol content, SR-mediated oxLDL uptake lacks negative feedback mechanisms and leads to uncontrolled oxLDL accumulation. These combined effects result in the conversion of macrophages to foam cells and the formation and buildup of plaque, where arteries become narrowed and hardened, which is one of the focal triggers for stroke, heart attack, or peripheral vascular disease [3, 4].

Conventional CVD therapeutics focus on lowering LDL cholesterol levels (e.g., statin) [5] or reducing plasma triglycerides (e.g., fibrates) [6], both of which contribute to atherosclerosis progression. Due to their systemic administration and their mechanisms of action, these therapies do not directly target atherosclerotic lesion sites and can lead to severe adverse effects (e.g., muscle damage, liver toxicity) [7, 8]. Consequently, novel drug targets including receptors and enzymes that are involved in signaling pathways and lipid metabolism at the sites of atherosclerotic plaque development have drawn tremendous interest over the last few decades [9]. An emerging strategy to abrogate the atherosclerotic cascade locally is through SR inhibition, by managing the disease from upstream events and preventing a series of pro-inflammatory events implicated in the incipient stages of the atherosclerotic cascade [10, 11]. For example, ApoE$^{-/-}$ mice with macrophages deficient in the expression of certain SRs (e.g., macrophage scavenger receptor 1 (MSR1) and cluster of differentiation 36 (CD36)) have demonstrated significant reduction (~80%) in lesion area of proximal aorta [12, 13].

Previously, our lab designed amphiphilic polymers (AMPs) consisting of a hydrophobically modified sugar backbone and a hydrophilic poly(ethylene glycol) (PEG) tail that modulated oxLDL uptake and trafficking in macrophages [14, 15]. By mimicking the anionic and hydrophobic characteristics of oxLDL and thus eliciting higher binding affinity to SRs, AMPs were designed and explored as SR inhibitors [16]. Subsequent *in vitro* studies revealed their strong potency to inhibit unregulated oxLDL uptake in macrophages primarily through competitive binding with SRs, particularly MSR1 and CD36. Furthermore, the AMP hydrophobic segment with unique 3D presentation served as the synthetic ligand binding domain for SRs, which is distinct from non-bioactive polymers (e.g., Pluronics) with similar composition [17]. Given their amphiphilicity, AMPs self-assemble into nanoscale micelles spontaneously in aqueous environments above their critical micelle concentrations (CMC), with a hydrophilic PEG corona preventing non-specific protein absorption during circulation [18, 19].

To deliver polymeric micelles effectively for biomedical applications, overcoming biological barriers *in vivo* such as serum instability and degradation susceptibility is prerequisite to fully achieving their therapeutic potential. Upon intravenous injection, AMP micelles undergo a drastic dilution in the bloodstream and are exposed to a variety of serum proteins, which induce micelle dissociation and reduce circulation time [20, 21]. Due to the fast clearance of unimers by renal filtration, a more stable form of AMPs is critical to enable longer blood circulation after intravenous injection and consequently enhanced accumulation in the vascular intima target sites [22]. Previous studies also indicated that the atheroprotective bioactivity of AMPs reported in the presence of serum can be significantly lower than serum-free conditions [23], which may be caused by competitive complexation with serum proteins (i.e., reduced bioavailability) [20]. Furthermore, a range of enzymes in the human body fluids are capable of catalyzing biomaterials hydrolysis, and their potential impact on AMP's plasma concentration or bioavailability must be considered [24]. A minimum effective concentration of AMPs is necessary to produce desirable anti-atherosclerotic potency. In view of the abundant presence of ester bonds within AMP structures (e.g., ester bond between sugar backbone and PEG), esterase-catalyzed AMP degradation could be particularly detrimental to their *in vivo* performance [14].

A rigorous evaluation of AMPs under biologically relevant conditions is critical to generate a more predictive model of the AMP potency *in vivo*. Building upon our previous work, three ester-linked AMPs and two ether-linked AMPs were synthesized with systematic modifications expected to enhance biological activity (Figure 1). A structure-activity relationship was developed, which correlated specific chemical features with anti-atherogenic properties as well as delivery efficacy under physiological conditions. Four parametric variations of chemical structure included were relative hydrophobicity, backbone stereochemistry, linkage type, and backbone presentation. The degree of oxLDL uptake in macrophages was quantified by incubating AMPs under both serum-free and serum-containing conditions. Solution properties of AMP micelles, such as CMC and half-life time ($t_{1/2}$) in serum, were carefully evaluated to predict their circulation behaviors *in vivo*. These experimental results were correlated to their respective 3D structures and evaluated by computational molecular simulations, which provide insights into key chemical attributes that not only elicit the intended bioactivity but also promote desirable physiochemical characteristics. Subsequently, the bioactivity of these AMPs in lipase-containing conditions was investigated by treating macrophages with AMPs that had previously been "conditioned" through exposure to lipase. Lastly, the stability of AMP micelles upon storage was assessed to evaluate their translational potential as bioactive formulations.

2. MATERIALS AND METHODS

2.1 Materials

All reagents and solvents were purchased from Sigma-Aldrich (Milwaukee, WI) and were used directly as received unless otherwise noted. Anhydrous dimethylformamide (DMF) was further dried over 4 Å molecular sieves overnight before use. Hydrochloric acid (HCl, 1 N), polytetrafluoroethylene (PTFE) syringe filters, and poly(vinylidene fluoride) (PVDF) syringe filters were purchased from Fisher Scientific (Fair Lawn, NJ). Di-*tert*-butyl *L*-

tartrate [25] and dimethyl amino pyridine p-toluene sulphonate (DPTS) [26] were prepared as previously published. Monomethoxy-poly(ethylene glycol) (PEG, 5 kDa) was azeotropically distilled with toluene (3× 50 mL) prior to use. For cell experiments, reagents include human buffy coats purchased from the Blood Center of New Jersey (East Orange, NJ) and New York Blood Center (Long Island City, NY), 1.077 g/cm^3 Ficoll-Paque Premium purchased from GE Healthcare (Pittsburgh, PA), RPMI 1640 from ATCC (Manassas, VA), macrophage colony stimulating factor (M-CSF) from PeproTech (Rocky Hill, NJ), fetal bovine serum (FBS) from Life Technologies (Grand Island, NY), 3,3'-dioctadecyloxacarbocyanine perchlorate (DiO) labeled oxLDL from Kalen Biomedical (Montgomery Village, MD), and unlabeled oxLDL from Biomedical Technologies Inc. (Stoughton, MA).

2.2 Characterization

Proton (^{1}H) and carbon (^{13}C) nuclear magnetic resonance (NMR) spectra were acquired on a Varian 400 or 500 MHz spectrophotometer. Samples were dissolved in deuterated chloroform (CDCl$_3$) with trimethylsilane (TMS) as an internal reference. Fourier transform infrared (FT-IR) spectra were recorded on a Thermo iS 10 FT-IR spectrometer using OMNI software as an average of 32 scans. FT-IR samples were prepared in CHCl$_3$ by solvent casting onto a sodium chloride (NaCl) plate. AMP precursor molecular weights (M_w) were determined by a ThermoQuest Finnigan LCQ-DUO system equipped with a syringe pump, an electrospray ionization (ESI) source, mass spectrometer (MS) detector, and the Xcalibur data system. Samples were prepared in spectrophotometric grade methanol (MeOH) at a concentration of 10 μg/ml. AMP weight average M_w and polydispersity indices (PDI) were determined by gel permeation chromatography (GPC) using a Waters LC system (Milford, MA) equipped with a 2414 refractive index detector, 1515 isocratic high performance liquid chromatography (HPLC) pump, 717plus autosampler, and a PLgel MIXED column (Agilent, Santa Clara, CA). Samples were prepared at 10 mg/mL in HPLC grade DCM and filtered through 0.45 μm PTFE syringe filters prior to injection at a flow rate of 1.0 mL/min. Broad molecular weight PEG standards (Waters, Milford, MA) were used for calibration. WaterBreeze v3.20 software was used for data collection and processing.

2.3 Synthesis

Amphiphilic polymers M12P5 [18], T12P5-meso [27], and T12P5-(L) [27] were prepared as previously published and discussed. These AMP systems are referred to as M12P5 or T12P5, in which M and T denotes mucic acid and tartaric acid, respectively, 12 refers to the number of carbon atoms of each aliphatic chain, P stands for PEG, and 5 indicates molecular weight of the PEG in kDa.

2.3.1 Synthesis of T(12-O)P5

DTT(12-O): Di-*tert*-butyl L-tartrate (DTT, 500 mg, 1.91 mmol) was dissolved in 15 mL anhydrous DMF and cooled to 0 °C using an ice bath. Sodium hydride (NaH, 160 mg, 4.00 mmol) was added subsequently and the reaction stirred for 20 min. Bromododecane (1.04 mL, 4.19 mmol) was added dropwise to the reaction via syringe pump. The reaction progress was monitored by silica gel thin layer chromatography (hexane: ethyl

acetate=85:15). After DTT was completely consumed, the reaction was allowed to stir for an additional 2 h before stopped. The reaction was quenched with saturated ammonium chloride (NH_4Cl) solution and extracted with ethyl acetate (3×20 mL). Organic layers were combined, washed with brine (1×60 mL), and dried over magnesium sulfate ($MgSO_4$) before solvent was removed *in vacuo*. DTT(12-O) was purified on silica gel via column chromatography using a hexane: ethyl acetate gradient (100:0 to 98:2). Yield: 548 mg, 48% (clear, colorless oil). ^{1}H-NMR (400 MHz, $CDCl_3$): 4.16 (s, 2H), 3.72 (m, 2H), 3.30 (m, 2H), 1.60 (m, 4H), 1.49 (s, 18H), 1.24 (b, 36H), 0.88 (t, 6H). ^{13}C-NMR (500 MHz, $CDCl_3$): 169.18, 81.93, 80.69, 72.68, 32.15, 29.87, 29.57, 28.37, 26.25, 22.91, 14.34. IR (cm^{-1}, thin film from $CHCl_3$): 1751 (C=O, ester), 1113 (C-O, ether). ESI-MS m/z: 621.4 $[M+Na]^+$.

T(12-O): DTT(12-O) (247 mg, 0.41 mmol) was dissolved in dichloromethane (DCM) under argon and cooled to 0 °C using an ice bath. Trifluoroacetic acid (TFA, 1.26 mL, 16.48 mmol) was then added dropwise via syringe and the reaction was stirred overnight. The reaction mixture was concentrated *in vacuo* and the pure product was precipitated in chilled hexane and collected via vacuum filtration. Yield: 182 mg, 91% (white powder). ^{1}H-NMR (400 MHz, $CDCl_3$): 4.38 (s, 2H), 3.69 (m, 2H), 3.53 (m, 2H), 1.60 (m, 4H), 1.25 (b, 36H), 0.88 (t, 6H). ^{13}C-NMR (500 MHz, $CDCl_3$): 172.49, 79.40, 73.64, 34.20, 31.90, 29.63, 29.61, 29.57, 29.49, 29.35, 29.33, 29.27, 25.72, 22.67, 14.10. IR (cm^{-1}, thin film from $CHCl_3$): 3500-3300 (OH, COOH), 1744 (C=O, COOH), 1165 (C-O, ether). ESI-MS m/z: 485.7 $[M-H]^-$.

T(12-O)P5: Following a published method, T(12-O) (136 mg, 0.28 mmol) and DPTS (24.5 mg, 0.25 mmol) were dissolved in 3 mL anhydrous DCM and 0.2 mL DMF. This solution was added to PEG (467 mg, 0.09 mmol). Once PEG was completely dissolved, N, N'-dicyclohexylcarbodiimide (DCC, 1 M in DCM, 0.29 mmol) was added dropwise via syringe and the reaction was stirred under argon. After 48 h, the reaction mixture was cooled to −20 °C to precipitate dicyclohexylurea (DCC) side product which was removed by vacuum filtration. The filtrate was washed with 0.1 N HCl (1×25 mL) and brine (2×25 mL). The combined organic layer was dried over $MgSO_4$, and concentrated *in vacuo*. The crude product was purified by precipitation into chilled diethyl ether and isolated via centrifugation (Hettich EBA 12, Beverly, MA; 3500 rpm, 3×5 min). Yield: 356 mg, 72% (white powder). ^{1}H-NMR (400 MHz, $CDCl_3$): 4.33 (b, 2H), 3.64 (b, ~ 500H), 1.64 (m, 4H), 1.25 (b, 36H), 0.88 (t, 6H). M_w, 5.2 kDa; PDI, 1.1.

2.3.2 Synthesis of T(12-O)P5$_{unsat}$

DBT(12-O)$_{unsat}$: Following a modified published procedure [28], a solution of dibenzyl L-tartrate (DBT, 661 mg, 2.00 mmol) and bromododecane (0.99 mL, 4.00 mmol) were dissolved in 10 mL anhydrous diethyl ether. Upon complete dissolution, silver (I) oxide (Ag_2O, 1.07 g, 4.60 mmol) was added and the reaction was refluxed in the dark at 47 °C for 72 h. The reaction mixture was filtered through a celite column and washed repeatedly with diethyl ether (3×10 mL). The combined filtrate was dried over $MgSO_4$, filtered, and pure product was precipitated from chilled hexane and isolated via vacuum filtration. Yield: 611 mg, 46%. ^{1}H-NMR (400 MHz, $CDCl_3$): 7.29 (b, 10H), 5.31 (s, 2H), 4.27 (t, 4H), 1.72 (m, 4H), 1.32 (b, 36H), 0.88 (t, 6H). ^{13}C-NMR (400 MHz, $CDCl_3$): 158.02, 134.46, 129.08,

128.93, 68.70, 67.55, 32.14, 29.83, 29.75, 29.66, 29.56, 29.36, 28.47, 25.90, 22.91, 14.60.
IR (cm^{-1}, thin film from $CHCl_3$): 3034 (C-H, Ar), 1743 (C=O, ester), 1260 (C-O, ether).
ESI-MS m/z: 687.4 $[M+Na]^+$.

T(12-O)$_{unsat}$: *DBT(12-O)$_{unsat}$* (481 mg, 0.72 mmol) was deprotected in the presence of
H_2(g) and 10 wt% palladium on carbon catalyst in anhydrous DCM (8 mL). The reaction
was stirred overnight and filtered through a celite column to remove catalyst. The filtrate
was concentrated *in vacuo* and dried over $MgSO_4$. Pure product was precipitated from
chilled hexane and collected via vacuum filtration. Yield: 297 mg, 85%. ^{1}H-NMR (500
MHz, $CDCl_3$): 4.28 (t, 4H), 1.75 (m, 4H), 1.38 (m, 4H), 1.26 (b, 32H), 0.88 (t, 6H). ^{13}C-
NMR (500 MHz, $CDCl_3$): 157.84, 157.1, 66.29, 30.91, 28.61, 28.54, 28.45, 28.33, 28.14,
27.21, 24.96, 24.65, 21.68, 13.09. IR (cm^{-1}, thin film from $CHCl_3$): IR (cm^{-1}, thin film
from $CHCl_3$): 3500-3100 (OH, COOH), 1743 (C=O, COOH), 1260 (C-O, ether). ESI-MS
m/z: 483.0 $[M-H]^-$.

T(12-O)P5$_{unsat}$: T(12-O)P5$_{unsat}$ was prepared in a similar manner as previously discussed
T(12-O)P5, using T(12-O)$_{unsat}$. Yield: 866mg, 72%. ^{1}H-NMR (400 MHz, $CDCl_3$): 4.43 (t,
2H), 4.28 (t, 2H), 3.64 (b, ~ 500H), 1.73 (m, 4H), 1.26 (b, 36H), 0.88 (t, 6H). M_w, 5.4 kDa;
PDI, 1.1.

2.4 Critical Micelle Concentration (CMC) Measurements

The CMC values of AMPs were determined by a pyrene assay as previously described [19].
A stock solution of pyrene was prepared in acetone at 1×10^{-7} M, and 0.5 mL of the solution
was transferred to a series of vials that were air dried overnight to evaporate the acetone.
AMPs were dissolved in HPLC grade water at 1×10^{-3} M and serial diluted to 1×10^{-4} –
1×10^{-10} M concentrations. For each concentration, 5 mL AMP solutions was added to the
vials with dried pyrene films. Pyrene was allowed to partition into AMP micelles by
incubation for 48 h at 37 °C with gentle agitation (60 RPM). Excitation measurements were
performed on a RF-5301PC spectrofluorometer (Shimadzu Scientific Instruments,
Columbia, MD) from 300 – 360 nm with 390 nm as the excitation wavelength. The
maximum emission wavelength of pyrene shifts from 332 nm to 334.5 nm upon its partition
into micelle's hydrophobic core in the excitation spectrum. The ratio of absorption of pyrene
in micelles (334.5 nm) to pyrene alone (332 nm) was plotted against the logarithm of AMP
concentrations and the inflection of the curve was taken as the CMC.

2.5 Dynamic Light Scattering (DLS) and Zeta Potential Measurements

DLS and zeta potential analysis were performed using a NanoZS90 instrument (Malvern
Instruments, Southboro, MA). Samples were dissolved in HPLC grade water at 2 mg/mL
and filtered using 0.45 μm PTFE syringe filters before each measurement. Each sample was
run at a 90° scattering angle in triplicate with 30 measurements per run at 25 °C. For micelle
stability stored at different conditions (4 °C and room temperature), AMPs were prepared at
10^{-3} M in PBS and sterilized by filtering through a 0.22 μm PVDF sterile syringe filters.
The micelle size and distribution were monitored by DLS over 2 months at predetermined
time points. All results were presented as mean ± standard deviation around the mean.

2.6 Isolation and Culture of Peripheral Blood Mononuclear Cells (PBMCs)

PBMCs were isolated from human buffy coats by Ficoll-Paque ($1.077g/cm^3$) density gradient. The red blood cell debris of red blood cells after lysing with ammonium-chloride-potassium (ACK) buffer and platelets were removed by centrifugation for 10 min. PBMCs were then washed with phosphate buffered saline (PBS) and transferred into T175 flasks (BD Falcon, Franklin lakes, NJ) containing 35 mL of base media (RPMI 1640 supplemented with 10% FBS and 1% penicillin/streptomycin). After 24 h incubation at 37 °C, adherent monocytes were selected and differentiated into human monocytes derived macrophages (HMDMs) by incubation in base media containing 50 ng/mL M-CSF for 7 days at 37 °C. The HMDMs were further plated at a concentration of 50,000 cells/well in 48-well plate for oxLDL uptake experiments.

2.7 OxLDL Uptake by Macrophages

The bioefficacy of AMPs (before or after enzyme degradation) was quantified by the inhibition of oxLDL uptake by HMDMs. HMDMs were incubated with unlabeled oxLDL (4 μg/mL) and fluorescent DiO labeled oxLDL (1 μg/mL) with or without AMPs (10^{-6} M and 10^{-7} M) in serum-free RPMI 1640 supplemented with 1% penicillin/streptomycin or RPMI 1640 supplemented with 10% FBS, 1% penicillin/streptomycin for 24 h. Treatments were then removed, replaced with cold PBS containing 2mM EDTA, and placed on ice packs. HMDMs were removed from plates by vigorous pipetting, transferred to 5 mL tubes, centrifuged at 1000 rpm for 10 min, and fixed in 1% paraformaldehyde (150 μL). Uptake of fluorescently labeled oxLDL was quantified using a FACScalibur flow cytometer (Becton Dickinson, Franklin Lakes, NJ) by collecting 10,000 events per sample and analyzed with FlowJo software (Tree Star Inc., Ashland, OR). The quantification of DiO fluorescence is represented by geometric mean fluorescence intensity (MFI). Results represented at least three independent experimental replicates. The bioefficacy of AMPs is presented by % oxLDL uptake, which was calculated using the following formula:

$$\% \quad \text{oxLDL} \quad \text{uptake} = 100 * \frac{MFI \quad of \quad AMP \quad containing \quad condition}{MFI \quad of \quad oxLDL \quad control}$$

2.8 Molecular Simulations

Molecular modeling calculations were performed on ester- and ether-linked AMP model compounds to evaluate similarities and differences in conformational preferences. All operations were conducted using the *Spartan'08* molecular modeling software suite (Version 4.0.0, Wavefunction, Inc., Irvine, CA). A total of five structures were constructed and explored, representing model compounds for the respective ester- and ether-based AMPs. For each model compound, simulations were performed on the neutral (-COOH) and anionic (-COO⁻) species. The anionic form depicts the putative state that would exist under physiological pH conditions (pH 7.4). The only structural modification for each compound was a truncated PEG domain to five ethylene oxide [-O-CH_2-CH_2-] units capped by a ethoxy [-O-CH_2-CH_3] terminal group. Preliminary calculations in which more PEG repeat units were added revealed insignificant impact on our findings (Figure S4) and, conversely, limited the number of physically meaningful conformers generated in conformational

searches. Molecular mechanics calculations were carried out using the Merck Molecular Force Field (MMFF) in an aqueous environment represented by the SM5.4 solvent model (MMFFaq). A stochastic search of conformational space was implemented on each molecule using a Monte Carlo (MC) procedure that generated 20,000 independent conformers, from which the equilibrium (lowest energy) conformers were selected for subsequent visual inspection. This MC scheme employed a simulated annealing algorithm that searched for the global low-energy conformer by biased sampling of low-energy conformers and high-energy conformers over the course of a step-wise descending temperature gradient.

2.9 Förster Resonance Energy Transfer (FRET) Pair Molecules Encapsulation

FRET pair containing micelles were prepared by the precipitation and membrane dialysis method [21]. AMPs (5 mg), 1,1'-dioctadecyl-3,3,3',3'-tetramethylindocarbocyanine perchlorate (DiI, 25 μg), and DiO (25 μg) were dissolved in 0.5 mL DMF and then diluted with 0.5 mL HPLC grade water. The solution was then dialyzed (Spectra/Por MWCO 3500) against 2 L distilled water for 2 days, where the water was changed every 2 h for the first 6 h. The micelle solution was filtered through a 0.45 μm PTFE syringe filters before use to remove unloaded FRET molecules.

2.10 FRET Fluorescence Spectroscopy

The fluorescence spectra of FRET experiments were performed on a RF-5301PC spectrofluorometer (Shimadzu Scientific Instruments, Columbia, MD) at an excitation wavelength of 484 nm, and the slit widths of excitation and emission were all fixed at 1.5 nm. Emission spectra were recorded from 490 to 590 nm.

The stability of AMP micelles (0.1 mg/mL) was studied in the presence of individual serum proteins and FBS at 37 °C. The concentrations of serum proteins tested were 45 mg/mL for albumin and 14 mg/mL for α and β globulins in PBS. Micelles were also diluted with PBS as a control to study the influence of dilution on micelle integrity. Time-resolved spectra were collected with an excitation wavelength at 484 nm and FRET ratio ($I_{565}/I_{565}+I_{501}$), where I_{565} and I_{501} are the fluorescence wavelength intensities of DiI and DiO, respectively, was calculated to monitor the disassociation of micelles every 10 min for 120 min [21].

2.11 Lipase Degradation of AMPs

AMPs were dissolved in PBS (pH=7.4) at 1×10^{-3} M and mixed with suspension of porcine pancreatic lipase at a final concentration of 12 U/mL. The solutions were then incubated at 37 °C with gentle agitation (60 rpm) for 24 h. The degradation media was extracted with DCM ($3 \times$ 10 mL) and solvent was removed *in vacuo*. AMP degradation products were redissolved in PBS for subsequent studies of oxLDL uptake in cells.

2.12 Statistical Analysis

All experiments were repeated in triplicate. OxLDL uptake results were analyzed by pairwise comparison with Dunnett's post hoc test using JMP® statistical software (SAS Institute Inc., Cary, NC). Significance criteria assumed a 95% confidence level ($p < 0.05$). Standard deviation is reported in the form of error bars.

3. RESULTS AND DISCUSSION

3.1 AMP Synthesis and Characterization

Five AMP structures were designed and selected with systematic variations to identify the critical chemical elements that influence bioactivity, serum stability, degradation stability, and storage stability. The hydrophobic domain size was varied to investigate the influence of hydrophobicity, while the backbone was altered to determine the role of stereochemistry and rigidity. In addition, linkage types between the backbone and hydrocarbon arms were investigated to study the effect on resultant molecular conformation, physicochemical properties, and bioactivity.

M12P5, T12P5-meso, and T12P5-(L) were prepared as previously published [18, 27]. The synthetic scheme of T(12-O)P5 has been reported previously; however, extremely low yield (~10%) for the alkylation step using dibenzyl L-tartrate has limited its further investigation and evaluation as an atherosclerotic therapeutic [14]. Herein, a new method using di-*tert*-butyl L-tartrate as a starting material for the alkylation was developed with significant yield improvement (~50%) and reduction of reaction time (Scheme 1). Trace amounts of sodium hydroxide was generated during the reaction as NaH reacts with residual water in the solvent, catalyzing benzyl group cleavage and leading to dibenzyl *L*-tartrate consumption. The sterically hindered *tert*-butyl esters minimized hydrolysis, resulting in improved efficiency. Following alkyl arm conjugation, DTT(12-O) was readily deprotected in the presence of strong acid TFA and subsequently subjected to carbodiimide catalyzed PEG coupling. A stoichiometric excess of diacid DTT(12-O) was used to ensure PEG only coupled to one side of the two carboxylic acids. The chemical compositions of AMP precursors were confirmed via NMR, FT-IR spectroscopies and MS, while the successful synthesis of mono-PEGylated AMP was verified by ^{1}H-NMR spectroscopy (i.e., AMP precursor to PEG ratio) and further confirmed with GPC (i.e., M_w).

To assess the influence of molecular conformation on bioactivity [29], the double bond that restricted rotational flexibility was introduced to the backbone and T(12-O)P5$_{unsat}$ was synthesized. Ag$_2$O served as both catalyst for ether formation [28] and oxidizing reagent [30] in the first step. The successful synthesis was indicated by the disappearance of the methine backbone peak (Figure S1). Hydrogenolysis was first attempted to deprotect benzyl groups of DBT(12-O) despite the presence of the unsaturated bond. Interestingly, the double bond was preserved, which is likely attributed to the steric hindrance caused by the bulky alkyl arms. Subsequent PEG coupling was accomplished with reasonably high yield (72 %).

Upon successful synthesis, the physicochemical properties of AMPs as micelles were evaluated in DI water at room temperature (Table 1). Micelle particle size, surface charge, and CMC values were determined, which are indicators of *in vivo* stability. To determine the applicability of these micellar systems for *in vivo* delivery, DLS was employed to measure micelle size. Furthermore, the morphology of micelles was characterized by transmission electron microscope (TEM). Notably, T(12-O)P5$_{unsat}$ exhibited a significant larger size compared to its flexible counterparts. This phenomenon likely due to the rigid hydrophobic domain, leading to a loose packing behavior of micelle hydrophobic core, as observed in molecular simulation. Computer snapshots of ether-linked AMPs T(12-O)P5 and T(12-

O)P5$_{unsat}$ in their respective low-energy conformations (Figure 2D and 2E) revealed improved alignment of the alkyl arms in the former than the latter. The arrangement is also reflected by the larger molecular volume and surface area of T(12-O)P5$_{unsat}$ (829 Å^3, 918 Å^2) compared with its flexible analogue T(12-O)P5 (742 Å^3, 824 Å^2) obtained from the simulations in anionic form (Table 2). All AMPs exhibited nanoscale sizes, ranging from 11 nm to 110 nm, which are considered optimal for extended blood circulation (10 – 200 nm) [22]. Despite variations sizes, AMP micelles were within the size range desirable for drug delivery applications (10 – 200 nm). TEM images provided a direct visualization of morphology of polymeric micelles and it is evident that micelles were prepared successfully with AMPs with an approximately spherical shape (Figure S3). Additionally, the zeta potential was evaluated as micelle colloidal stability is partially attributed to electrostatic repulsion arising from the net surface charge of the particles [31]. AMP micelles exhibited slightly negative charge (~ −1.1 – −2.3 mV), demonstrating a similar degree of electronic stabilization effect.

CMC is defined as the concentration above which unimer (i.e., individual AMP molecules) self-assemble into micelles spontaneously, and is assessed by a well-established pyrene assay [18, 19]. Micelles undergo tremendous environmental changes upon intravenous administration, including extensive dilution, leading to dissociation of micelles into unimer form. Low CMC values imply that micelles maintain better integrity upon drastic dilution in the bloodstream, which is beneficial for *in vivo* delivery. Among all formulations tested, mucic acid-derived M12P5 had a CMC value one or two orders-of-magnitude lower than tartaric acid-derived AMP micelles, implying a better stability towards dilution. As the micellization process is driven by hydrophobic interactions [32], the observed difference in CMC likely stems from M12P5 having a larger hydrophobic domain (4 hydrocarbon arms) than tartaric-acid based AMPs (2 hydrocarbon arms), resulting in a stronger hydrophobic interaction. This observation is confirmed by calculated values of the non-polar surface area (NPSA) of the low-energy conformers (Table 2), indicating the hydrophobicity of AMPs. Specifically, the NPSA is at least 50% larger for M12P5 compared with the other four AMPs considered in this study. Overall, all AMPs exhibited very low CMC values (10^{-7} – 10^{-5} M) compared to current drug delivery systems under investigation [33, 34], suggesting their promise for drug delivery applications.

3.2 AMP Biological Activity

Despite the importance of administering AMPs above their CMC to ensure successful delivery in a biological setting, micelle form has a minimal influence on the corresponding anti-atherosclerotic activity compared to chemical composition, as shown previously [35]. To evaluate the influence of single chemical structure changes on bioactivity, HMDMs were first coincubated with AMPs at 10^{-6} M and fluorescently-labeled oxLDL for 24 h under serum-free conditions, after which oxLDL uptake was quantified with flow cytometry (Figure 1). It has been previously demonstrated and further confirmed herein that oxLDL uptake level was markedly reduced with 10^{-6} M M12P5 treatment (~17%), and thus, M12P5 is referred to as the "gold standard" [17]. Compared to M12P5, T12P5-meso with reduced hydrophobicity exhibited a comparable effect on oxLDL uptake inhibition effect (~ 27%), suggesting that hydrophobicity is not the exclusive determinant of bioactivity. However,

T12P5-(L) with differing backbone stereochemistry compared to T12P5-meso, presented little inhibitory effect and oxLDL uptake remained as high as 78%, demonstrating that sugar backbone stereochemistry is critical to enhance bioactivity. To examine the effect of linkage type and backbone flexibility, T(12-O)P5 was compared to T12P5-(L) and T(12-O)P5$_{unsat}$, respectively. Replacing the ester linkage with ether linkage, T(12-O)P5 inhibited oxLDL uptake to a greater extent and lowered levels of intracellular oxLDL to nearly basal levels (~ 10%). In contrast, the introduction of a rigid functionality into the sugar backbone did not elicit enhancement of bioactivity. In fact, *trans* T(12-O)P5$_{unsat}$ showed no bioactivity compared to the oxLDL-only control group (i.e., no AMP treatment). Collectively, these results highlight the key criteria for bioactivity: backbone stereochemistry, linkage type, and molecular conformation conferred by backbone presentation. Overall, M12P5, T12P5-meso, and T(12-O)P5 significantly reduced cellular uptake of oxLDL in macrophages to basal level.

To mimic physiological conditions, AMP's ability to block oxLDL uptake under serum-containing conditions was also investigated. However, at the same concentration (10^{-6} M), all AMPs lost their biological activity in the presence of serum proteins. Similar observations were reported in the literature with other therapeutics, which may result from serum protein interactions with drugs. Therefore, AMPs were further studied at a higher concentration (10^{-5} M) in the presence of serum. An overall improvement of oxLDL uptake inhibition potency was observed, suggesting a strong concentration-dependent effect of AMPs. Although both M12P5 and T12P5-meso were able to significantly lower oxLDL internalization, M12P5 (28%) was twice as efficacious as the less hydrophobic analog T12P5-meso (57%), indicating the potential impact of hydrophobicity on enhanced bioactivity under serum-containing conditions. As previously shown by Gao *et al.* [36], increased polymer hydrophobicity leads to increase in both the tendency to form polymeric micellar aggregates and to bind to serum proteins. Given our results, it is plausible that enhanced hydrophobic interactions within the M12P5 micellar core prevents AMPs from binding with serum proteins. Meanwhile, T(12-O)P5 was able to effectively impede oxLDL uptake and maintained the nearly basal levels, implying its potential benefits for *in vivo* use. Thus, the structure-activity relationship trends observed in serum-containing conditions parallels those of serum-free conditions except for the role of hydrophobicity.

Lead AMPs selected through *in vitro* cell study based on oxLDL uptake inhibitory efficacy, including M12P5, T12P5-meso, and T(12-O)P5, were further studied in terms of serum stability, degradation stability, and storage stability for viability as atherosclerotic therapeutic candidates.

3.3 Molecular Simulations

To further elucidate the solution behavior as well as biological activity of the AMPs, we evaluated the influence of varied structural features on the molecular conformation of the hydrophobic core domains, given that hydrophobic interactions are the main driving force for micellization as well as anti-atherosclerotic bioactivity via enhanced binding with SRs [35]. We adapted a previously established molecular modeling framework and compared the conformational features and overall molecular architectures of the selected AMPs that share

the same alkyl arm length but differ with respect to their stereochemistry, linkage (ester vs. ether), and sugar backbone (mucic vs. tartaric acid). MC simulations were performed on model compounds of the five subject AMPs to identify the low-energy conformer and calculate selected biophysical properties, i.e., dipole moment, molecular volume (Mol Vol), total surface area (TSA), polar surface area (PSA), non-polar surface area (NPSA), and the average C...C distance between the neighboring alkyl arms ($<C...C>_{avg}$). These values were tabulated for the AMPs simulated as both uncharged (Table S1) and anionic species (Table 2). Snapshots of the calculated low-energy conformer for each anionic species are presented in Figure 2.

Some generalizations were established between individual AMPs. The calculated dipole moments are far larger in magnitude for the anionic analogs (range 23 –34 Debye) than for their uncharged counterparts (range 2.6 – 4.8 Debye). This finding is a direct consequence of greater polarity of free negative charge on the carboxylate moiety of anionic analogs.

In all cases, except for T(12-O)P5$_{unsat}$, the neighboring alkyl arms are relatively aligned as reflected in the $<C...C>_{avg}$ distance, which ranged from 4.0 Å to 6.2 Å for these structures. T(12-O)P5$_{unsat}$ did not fit this pattern, with a $<C...C>_{avg}$ distance at 10 – 15 Å. As suggested by the snapshots (Figure 2E), this high value stems from the *trans* C=C configuration which effectively directs the neighboring alkyl arms in opposite directions. Collectively, the dipole moments of these structures reflect their amphiphilic nature, as the primary driving force for micelle formation.

The differences in rotational flexibility between the corresponding linkers of the ester-linked T12P5-L (27.2 Debye) and the ether-linked T(12-O)P5 (23.2 Debye) result in a clear disparity in dipole moment. The ether linkage is relatively small and flexible, which allows the two alkyl arms to adopt a compact parallel alignment (Figure 2D), while the ester linkage is rotationally less flexible. Moreover, the ester dipoles adopt an antiparallel orientation that directs the alkyl arms in divergent directions (Figure 2B). These observations are supported by the CMC values in which better alignment of the ether-linked T(12-O)P5 correlates with a lower CMC value compared to ester-linked T12P5-L (Table 1). As noted above, the low-energy conformer of T(12-O)P5$_{unsat}$ obtained from the molecular simulations features the two alkyl arms pointing in opposite directions. This feature is also quantified by the substantial difference in the $<C...C>$ distance between the alkyl arms for T(12-O)P5$_{unsat}$ and its flexible analog T(12-O)P5 and as neutral (15 Å vs. 5 Å) or as anionic (10.3 Å vs. 4.4 Å) species. This structural arrangement is not expected to be conducive to micelle stabilization as supported by T(12-O)P5$_{unsat}$'s highest CMC value. M12P5, which has the lowest CMC value among these five AMPs (Table 1), has the highest value of the calculated total surface area and non-polar surface area yet only a moderate dipole moment (32 Debye) as a negatively charged species (Table 2). The simulation results highlighted the significant influence of minute structural changes of AMPs on their corresponding solution properties.

Apart from the aggregation behavior, the 3D molecular modeling also provides invaluable insights into AMPs' biological properties. Due to the presence of hydrophobic residues within the SR binding pockets, hydrophobic interaction has been shown to play a crucial

role in determining the resultant oxLDL uptake inhibition efficiency. Thus, the superior bioactivity of T(12-O)P5 was likely a result of tightly packed hydrophobic domain as suggested by its small dipole and short $<C...C>_{avg}$ distance. In contrast, T(12-O)P5$_{unat}$ with alkyl arms in opposite directions largely eliminates the potential coordinative effects between arms to enhance binding affinity to SRs, leading to a markedly reduced bioactivity compared to its counterparts.

3.4 AMP Serum Stability

The integrity of AMP micelles upon incubation with serum was examined, providing insights into micelle circulation stability in blood, as sufficiently long blood circulation time allows prolonged access to and efficient accumulation at disease sites. Here, FRET pair (DiO and DiI) encapsulated micelles were explored to estimate their serum stability. Unlike attaching a fluorophore to polymeric micelles as a marker, which invariably alters micelle behavior, using a FRET-based method is a more accurate approach to evaluate micellar integrity without chemically modifying polymers' structure. When both FRET molecules were loaded inside one micelle and excited at 484 nm, a strong emission of DiI at 565 nm was observed as a result of energy transfer between DiO and DiI. Upon micelle dissociation, the FRET molecules were released and diffused apart, eliminating the energy transfer and leading to a shift of emission peak from 565 (DiI) to 501 nm (DiO). Therefore, micelle disassembly was characterized by the decrease in the FRET ratio ($I_{565}/I_{565}+I_{501}$).

PBS alone was first added to AMP micelles as a control to identify the impact of dilution during the experiment concurrently in addition to protein disruption. Minimal FRET ratio changes were shown for all three AMP micelles (Figure 3), indicating the dilution factor had little, if any, influence on micelle destabilization. This result further validated the benefits of using AMPs with low CMC values as carriers. Micelles were then incubated with FBS at 37 °C to represent the physiological conditions. In contrast, a FRET ratio decrease was observed upon incubation with FBS over time in an exponential manner. Due to hydrophobic interactions, serum proteins were determined to be the major factor that led to the micelle disassembly. The FRET ratio underwent a rapid initial decrease, which suggested the fast release of encapsulated FRET molecules from micellar core and finally reached a plateau value as micelles became fully disassembled. The $t_{1/2}$ value is defined as the time required for half of the micelles to disassemble. Because of the linear correlation between FRET ratio and percentage of disassembled micelles demonstrated by Lu *et al.* previously [21], the $t_{1/2}$ of AMP micelles in FBS was estimated as the time required to reach midpoint of the initial FRET ratio and the plateau of the FRET ratio. M12P5 exhibited a $t_{1/2}$ of 30 min, which was much longer than any of the tartaric-based AMPs micelles (10 min). This effect is likely due to the stronger hydrophobic interaction of M12P5 alkyl arms in the micellar core, withstanding the serum protein-induced micelle destabilization. Although T(12-O)P5 and T12P5-meso were similar in hydrophobicity, T(12-O)P5 had a $T_{1/2}$ time slightly longer than T12P5-meso.

To further explore the influence of individual proteins present in serum on micelle integrity, FRET experiments with albumin and α and β globulins were conducted. While albumin was chosen due to its abundance (approximately 60 %) in serum, α and β globulins were chosen

based upon their potential to destabilize micelles. The concentrations of serum albumin (45 mg/mL) and α and β globulins (14 mg/mL) in PBS were selected based on average plasma concentrations [37]. M12P5 micelles exhibited robust stability towards albumin disruption during incubation, as only a slight decrease in the FRET ratio was detected. In contrast, the FRET ratio decreased drastically for both T(12-O)P5 and T12P5, suggesting that they were more likely to lose their integrity in the presence of albumin compared to M12P5. Incubation with α and β globulins significantly lowered the FRET ratio of AMP micelles to 0.58, 0.53, and 0.52 for M12P5, T12P5, and T(12-O)P5, respectively, over 2 h. The faster FRET ratio decrease compared to albumin conditions indicated that α and β globulins were the primary factors in serum responsible for the rapid compromise of micelle integrity, consistent with observation reported by Diezi *et al* [37].

3.5 AMP Degradation Stability

Metabolic instability, particularly susceptibility to enzyme-catalyzed degradation, has long been considered a primary factor responsible for the high failure rate of drug candidates translating from *in vitro* work to clinical phase [38]. Previously, we examined the chemical composition change of AMPs upon incubation with lipase solution over 24 h via ^{1}H-NMR. While lauric acid and PEG were detected as degradation products of ester-linked AMPs, ether-linked AMPs were shown to have intact hydrophobic segment with only PEG cleavage [19]. Herein, we further studied how AMP degradation alters their respective bioactivity *in vitro* by treating HMDMs with degraded AMPs reconstituted in PBS buffer at predetermined concentrations under serum-free conditions (Figure 4). Degraded AMPs were extracted from degradation media with DCM and redissolved in PBS, assuring the complete removal of water soluble lipase, which may influence subsequent oxLDL uptake study.

As shown in Figure 4, degraded AMPs were approximately 3 – 4 fold less efficacious at reducing oxLDL accumulation compared to undegraded AMPs at 10^{-6} M. As expected, lipase-catalyzed ester degradation significantly decreased effective AMP concentration, leading to compromised efficacy. In fact, minimal residual bioactivity was detected as oxLDL uptake as high as 73% and 88% was observed for the ester-linked AMPs, M12P5 and T12P5-meso, respectively. It is noteworthy that ether-linked AMP T(12-O)P5 was still able to suppress oxLDL uptake levels to as low as 44% after 24 h lipase incubation, which was significantly better than when treated with ester-linked AMPs. This phenomenon likely resulted from enhanced metabolic stability conferred by ether linkage as previously discussed [14]. This result further validated the necessity of improving enzymatic degradation stability for enhanced bioactivity *in vivo*. When administered at 10^{-5} M, all AMPs remarkably repressed the oxLDL uptake, particularly with T(12-O)P5 to a basal level.

Collectively, these results demonstrate that lipase remarkably compromised AMPs' bioactivity and the introduction of ether linkages dramatically improve the degradation stability of T(12-O)P5, contributing to a potential enhanced anti-atherosclerotic efficacy *in vivo*.

3.6 AMP Storage Stability

Micelle stability at different storage conditions (room temperature and 4°C) was evaluated to test the viability of AMP micellar assemblies as cardiovascular therapeutic candidates. Despite easy preparation of micellar delivery system compared to other widely used formulations (e.g., liposome, nanoparticle, etc.), micelles are usually prone to aggregation during storage due to their dynamic nature [39].

Upon storage at either room temperature or 4 °C, the colloidal stability of AMP micelles was monitored by tracking particle size and size distribution at 10^{-3} M, which is representative of typical storage concentration, by DLS over 2 months (Figure 5). No precipitation was visually observed for any selected formulations at either temperature during the monitored period. While T12P5-meso and T(12-O)P5 exhibited negligible size changes as well as slight size distribution change, M12P5 maintained a relative constantly size but with large size variations (up to ± 7 nm). Meanwhile, aggregation peaks started to appear above 2000 nm after week 1 and gradually resulted in the reduction of peak intensity (room temperature to 84% and 4 °C to 93% by week 8). Overall, these results indicated that both T12P5-meso and T(12-O)P5 micelles were physically stable under storage temperatures for at least 2 months.

4 CONCLUSION

Three ester-linked AMPs and two ether-linked AMPs were synthesized and assessed comprehensively to reveal their anti-atherosclerotic potency, including oxLDL uptake inhibition, serum stability, degradation stability, and storage stability. Minor chemical modifications induced significant changes in biological activity as well as physicochemical properties. Particularly, ether linkages between the hydrophobic arms and the sugar backbone dramatically enhanced AMP's bioactivity, degradation stability, and storage stability compared to ester linkage. This effect is likely due to the enhanced alignment within the hydrophobic domain, as indicated by 3D modeling results, as well as enhanced metabolic stability. Event though T(12-O)P5 micelles tend to be less stable during in the presence of serum, kinetically assembled nanoparticles can be prepared with improved resistance to serum disruption. While lipid-lowering treatments (e.g., statin) are effective when prescribed for treating CVD in the early stages, new therapeutic approaches like targeting SRs are more powerful to control the progression of the disease. Overall, T(12-O)P5 was synthesized with greatly improved yield and identified as a lead candidate molecule that will be investigated further *in vivo*. As enzyme-catalyzed degradation was shown to markedly compromise AMP's bioactivity, replacing the ester linkage between the hydrophobic domain and PEG tail with more robust amide linkage, by using amine-terminated PEG, is expected to further improve their efficiency *in vivo*.

Supplementary Material

Refer to Web version on PubMed Central for supplementary material.

ACKNOWLEDGMENTS

REFERENCES

1. Mozaffarian D, Benjamin EJ, Go AS, Arnett DK, Blaha MJ, Cushman M, et al. Heart disease and stroke statistics-2015 update: a report from the american heart association. Circulation. 2015; 131:e29. [PubMed: 25520374]

2. Chnari E, Lari HB, Tian L, Uhrich KE, Moghe PV. Nanoscale anionic macromolecules for selective retention of low-density lipoproteins. Biomaterials. 2005; 26:3749–58. [PubMed: 15621265]

3. Patel RP, Moellering D, Murphy-Ullrich J, Jo H, Beckman JS, Darley-Usmar VM. Cell signaling by reactive nitrogen and oxygen species in atherosclerosis. Free Radical Biology and Medicine. 2000; 28:1780–94. [PubMed: 10946220]

4. Chnari E, Nikitczuk JS, Uhrich KE, Moghe PV. Nanoscale Anionic Macromolecules Can Inhibit Cellular Uptake of Differentially Oxidized LDL. Biomacromolecules. 2006; 7:597–603. [PubMed: 16471936]

5. Stroes E. Statins and LDL-cholesterol lowering: an overview. Current Medical Research and Opinion. 2005; 21:S9–S16. [PubMed: 16138936]

6. Staels B, Dallongeville J, Auwerx J, Schoonjans K, Leitersdorf E, Fruchart J-C. Mechanism of Action of Fibrates on Lipid and Lipoprotein Metabolism. Circulation. 1998; 98:2088–93. [PubMed: 9808609]

7. Golomb BA, Evans MA. Statin Adverse Effects: A Review of the Literature and Evidence for a Mitochondrial Mechanism. American journal of cardiovascular drugs : drugs, devices, and other interventions. 2008; 8:373–418.

8. Elisaf M, Florentin M, Liberopoulos E, Mikhailidis D. Fibrate-associated adverse effects beyond muscle and liver toxicity. Current pharmaceutical design. 2008; 14:574–87. [PubMed: 18336300]

9. Jamkhande PG, Chandak PG, Dhawale SC, Barde SR, Tidke PS, Sakhare RS. Therapeutic approaches to drug targets in atherosclerosis. Saudi Pharmaceutical Journal. 2014; 22:179–90. [PubMed: 25061401]

10. Moore KJ, Freeman MW. Scavenger Receptors in Atherosclerosis: Beyond Lipid Uptake. Arteriosclerosis, Thrombosis, and Vascular Biology. 2006; 26:1702–11.

11. Boullier A, Bird DA, Chang M-K, Dennis EA, Friedman P, Gillotte-Taylor K, et al. Scavenger Receptors, Oxidized LDL, and Atherosclerosis. Annals of the New York Academy of Sciences. 2001; 947:214–23. [PubMed: 11795269]

12. Babaev VR, Gleaves LA, Carter KJ, Suzuki H, Kodama T, Fazio S, et al. Reduced Atherosclerotic Lesions in Mice Deficient for Total or Macrophage-Specific Expression of Scavenger Receptor-A. Arteriosclerosis, Thrombosis, and Vascular Biology. 2000; 20:2593–9.

13. Febbraio M, Podrez EA, Smith JD, Hajjar DP, Hazen SL, Hoff HF, et al. Targeted disruption of the class B scavenger receptor CD36 protects against atherosclerotic lesion development in mice. The Journal of Clinical Investigation. 2000; 105:1049–56. [PubMed: 10772649]

14. Abdelhamid DS, Zhang Y, Lewis DR, Moghe PV, Welsh WJ, Uhrich KE. Tartaric acid- based amphiphilic macromolecules with ether linkages exhibit enhanced repression of oxidized low density lipoprotein uptake. Biomaterials. 2015; 53:32–9. [PubMed: 25890704]

15. Gu L, Faig A, Abdelhamid D, Uhrich K. Sugar-Based Amphiphilic Polymers for Biomedical Applications: From Nanocarriers to Therapeutics. Accounts of chemical research. 2014; 47:2867–77. [PubMed: 25141069]

16. Wang J, Plourde NM, Iverson N, Moghe PV, Uhrich KE. Nanoscale amphiphilic macromolecules as lipoprotein inhibitors: the role of charge and architecture. International Journal of Nanomedicine. 2007; 2:697–705. [PubMed: 18203436]

17. Chnari E, Nikitczuk JS, Wang J, Uhrich KE, Moghe PV. Engineered Polymeric Nanoparticles for Receptor-Targeted Blockage of Oxidized Low Density Lipoprotein Uptake and Atherogenesis in Macrophages. Biomacromolecules. 2006; 7:1796–805. [PubMed: 16768400]

18. Tian L, Yam L, Zhou N, Tat H, Uhrich KE. Amphiphilic Scorpion-like Macromolecules: Design, Synthesis, and Characterization. Macromolecules. 2004; 37:538–43.

19. Abdelhamid D, Arslan H, Zhang Y, Uhrich KE. Role of branching of hydrophilic domain on physicochemical properties of amphiphilic macromolecules. Polymer Chemistry. 2014; 5:1457–62. [PubMed: 24533034]

20. Miller T, Rachel R, Besheer A, Uezguen S, Weigandt M, Goepferich A. Comparative Investigations on In Vitro Serum Stability of Polymeric Micelle Formulations. Pharm Res. 2012; 29:448–59. [PubMed: 21879388]

21. Lu J, Owen SC, Shoichet MS. Stability of Self-Assembled Polymeric Micelles in Serum. Macromolecules. 2011; 44:6002–8. [PubMed: 21818161]

22. Kim S, Shi Y, Kim JY, Park K, Cheng J-X. Overcoming the barriers in micellar drug delivery: loading efficiency, in vivo stability, and micelle–cell interaction. Expert Opinion on Drug Delivery. 2009; 7:49–62. [PubMed: 20017660]

23. Iverson NM, Sparks SM, Demirdirek B, Uhrich KE, Moghe PV. Controllable inhibition of cellular uptake of oxidized low-density lipoprotein: Structure–function relationships for nanoscale amphiphilic polymers. Acta Biomaterialia. 2010; 6:3081–91. [PubMed: 20170758]

24. Azevedo, HS.; Reis, RL. Biodegradable systems in tissue engineering and regenerative medicine. CRC Press; Boca Raton, FL: 2005. Understanding the enzymatic degradation of biodegradable polymers and strategies to control their degradation rate.; p. 177201

25. Uray G, Lindner W. tert-butyl esters and ethers of (R,R)-tartaric acid. Tetrahedron. 1988; 44:4357–62.

26. Moore JS, Stupp SI. Room temperature polyesterification. Macromolecules. 1990; 23:65–70.

27. Poree DE, Zablocki K, Faig A, Moghe PV, Uhrich KE. Nanoscale Amphiphilic Macromolecules with Variable Lipophilicity and Stereochemistry Modulate Inhibition of Oxidized Low-Density Lipoprotein Uptake. Biomacromolecules. 2013; 14:2463–9. [PubMed: 23795777]

28. Aurich HG, Biesemeier F. Intramolecular 1, 3-Dipolar cycloaddition of transient enantiomerically pure oxaalkenyl nitrones. Synthesis. 1995:1171–8.

29. Hehir S, Plourde NM, Gu L, Poree DE, Welsh WJ, Moghe PV, et al. Carbohydrate composition of amphiphilic macromolecules influences physicochemical properties and binding to atherogenic scavenger receptor A. Acta Biomaterialia. 2012; 8:3956–62. [PubMed: 22835678]

30. Iyer MR, Trivedi GK. Silver(I) Oxide Catalyzed Oxidation of o-Allyl- and o-(1-Propenyl)phenols. Bulletin of the Chemical Society of Japan. 1992; 65:1662–4.

31. Olsen SN, Andersen KB, Randolph TW, Carpenter JF, Westh P. Role of electrostatic repulsion on colloidal stability of Bacillus halmapalus alpha-amylase. Biochimica et Biophysica Acta (BBA) - Proteins and Proteomics. 2009; 1794:1058–65. [PubMed: 19281873]

32. Israelachvili J, Pashley R. The hydrophobic interaction is long range, decaying exponentially with distance. Nature. 1982; 300:341–2. [PubMed: 7144887]

33. Samith VD, Miño G, Ramos-Moore E, Arancibia-Miranda N. Effects of pluronic F68 micellization on the viability of neuronal cells in culture. Journal of Applied Polymer Science. 2013; 130:2159–64.

34. Alexandridis P, Holzwarth JF, Hatton TA. Micellization of Poly(ethylene oxide)- Poly(propylene oxide)-Poly(ethylene oxide) Triblock Copolymers in Aqueous Solutions: Thermodynamics of Copolymer Association. Macromolecules. 1994; 27:2414–25.

35. Faig A, Petersen LK, Moghe PV, Uhrich KE. Impact of Hydrophobic Chain Composition on Amphiphilic Macromolecule Antiatherogenic Bioactivity. Biomacromolecules. 2014; 15:3328–37. [PubMed: 25070717]

36. Gao JY, Dubin PL. Binding of proteins to copolymers of varying hydrophobicity. Biopolymers. 1999; 49:185–93. [PubMed: 10070266]

37. Diezi TA, Bae Y, Kwon GS. Enhanced Stability of PEG-block-poly(N-hexyl stearate l aspartamide) Micelles in the Presence of Serum Proteins. Molecular Pharmaceutics. 2010; 7:1355–60. [PubMed: 20575526]

38. Nassar A-EF, Kamel AM, Clarimont C. Improving the decision-making process in the structural modification of drug candidates: enhancing metabolic stability. Drug Discovery Today. 2004; 9:1020–8. [PubMed: 15574318]

39. Musacchio T, Laquintana V, Latrofa A, Trapani G, Torchilin VP. PEG-PE micelles loaded with paclitaxel and surface-modified by a PBR-ligand: synergistic anticancer effect. Molecular pharmaceutics. 2009; 6:468–79. [PubMed: 19718800]
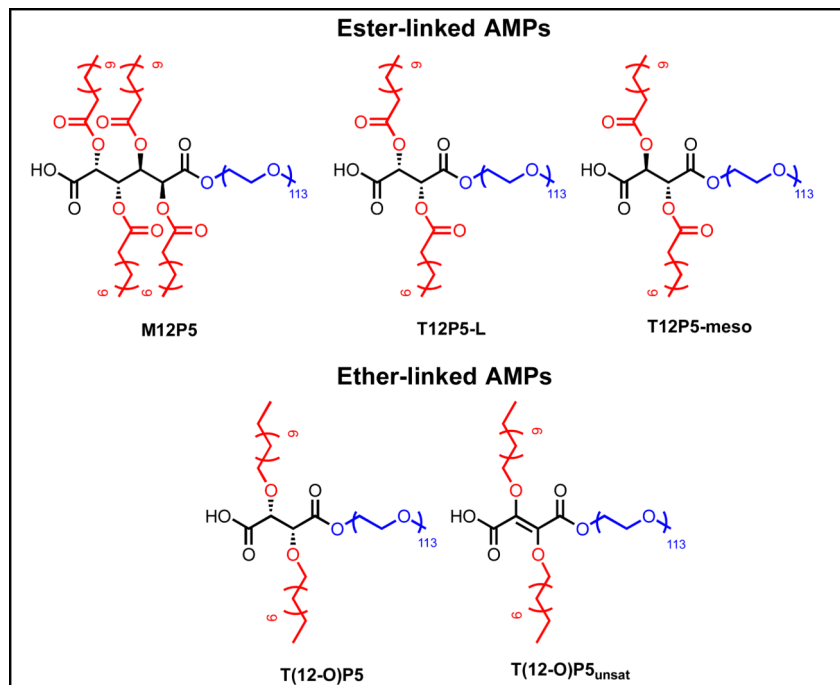
Figure 1.
Chemical structures of ester-linked AMPs and ether-linked AMPs. AMPs were designed to investigate the role of chemical composition on serum and degradation stability as well as atheroprotective bioactivity. The sugar backbones (black) and hydrophobic arms (red) together confer bioactivity in terms of binding to scavenger receptors for blockage of oxLDL uptake.
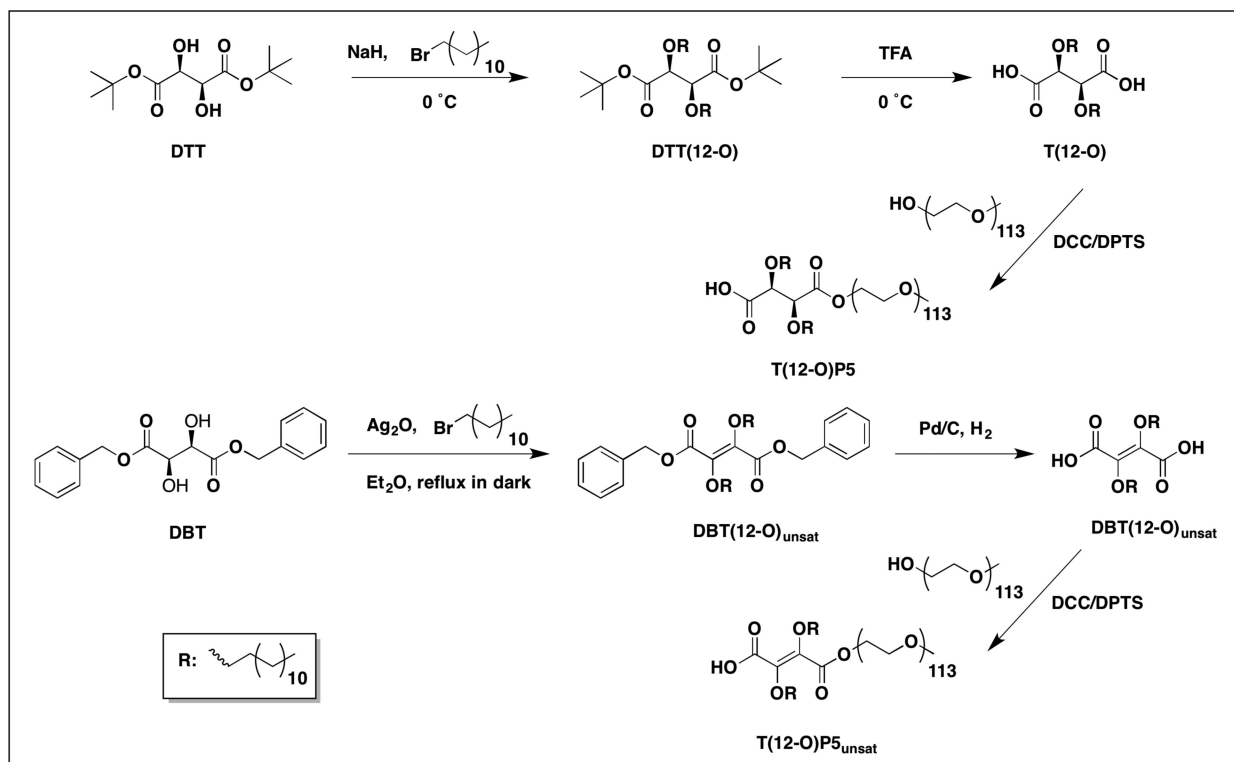
Scheme 1.
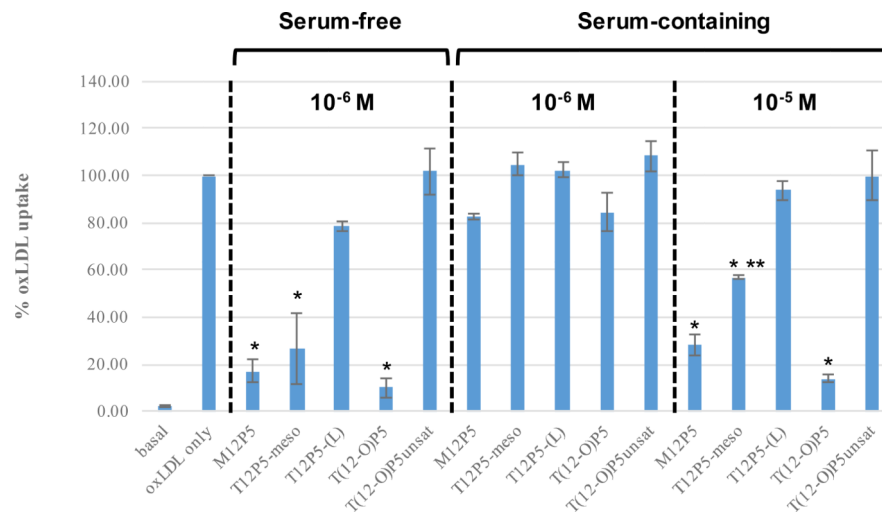Synthetic scheme of ether-linked AMPs T(12-O)P5 and T(12-O)P5$_{unsat}$.

Figure 1.
Effect of serum and concentration on AMP's oxLDL uptake inhibitory effects. HMDMs treated with AMPs under the same condition (i.e., concentration and serum presence or absence) are grouped between dashed lines. The single asterisk (*) represents a significant difference from the positive oxLDL only control. The double asterisk (**) indicates significant difference compared to M12P5 and T(12-O)P5 at 10^{-5} M under serum-containing conditions.
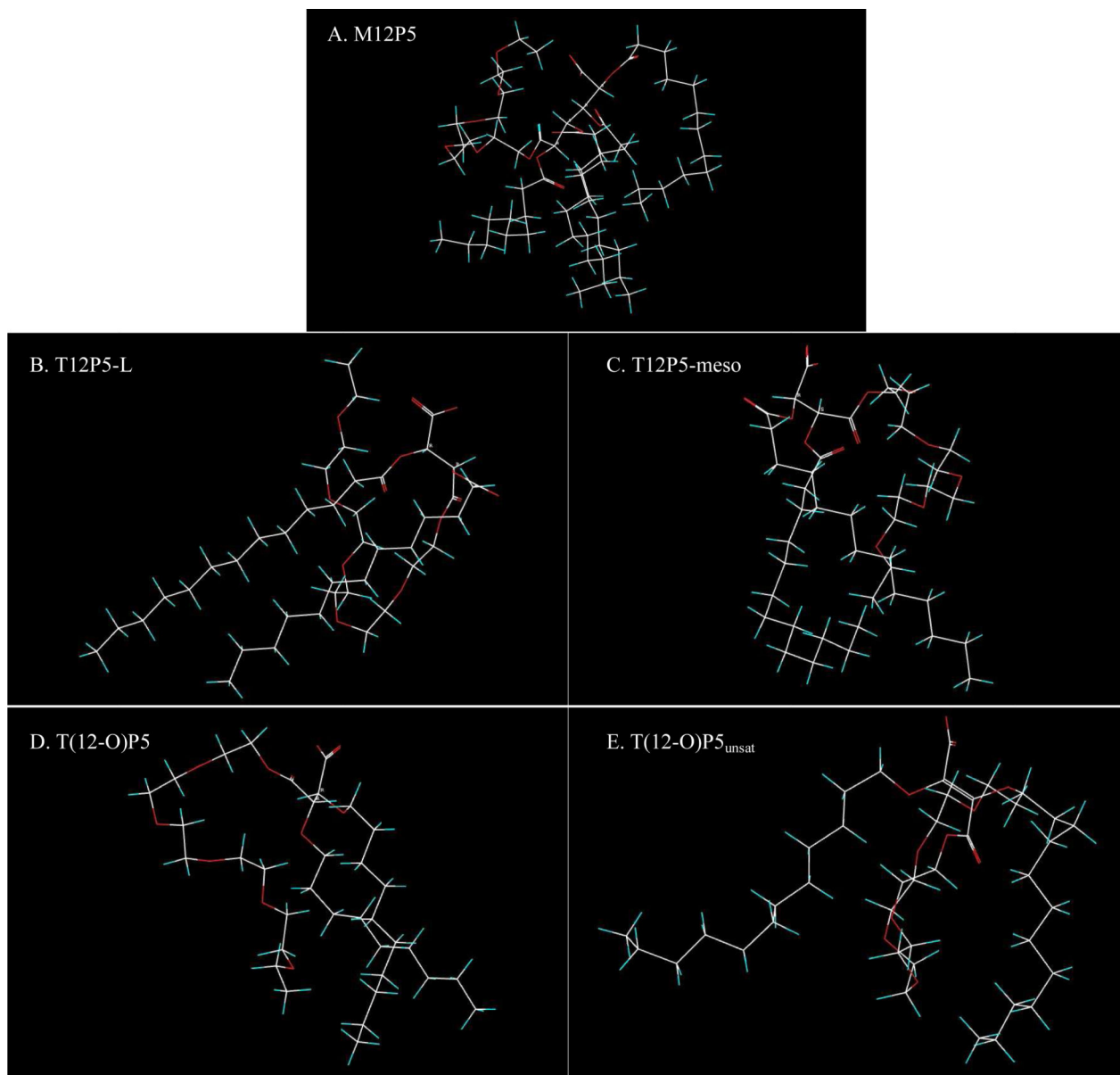
Figure 2.
Computer snapshots of equilibrium (low-energy) conformer of the AMPs as anionic species from MC simulations. Atoms are color-coded: C (white), H (green), O (red). All the structures depicted in the figure are oriented such that their dipole moment is aimed in the vertical direction with the negative pole pointing upward. Inspection of each structure reveals that there is a distinct separation between the hydrophilic groups (carboxyl and PEG) and the hydrophobic arms.
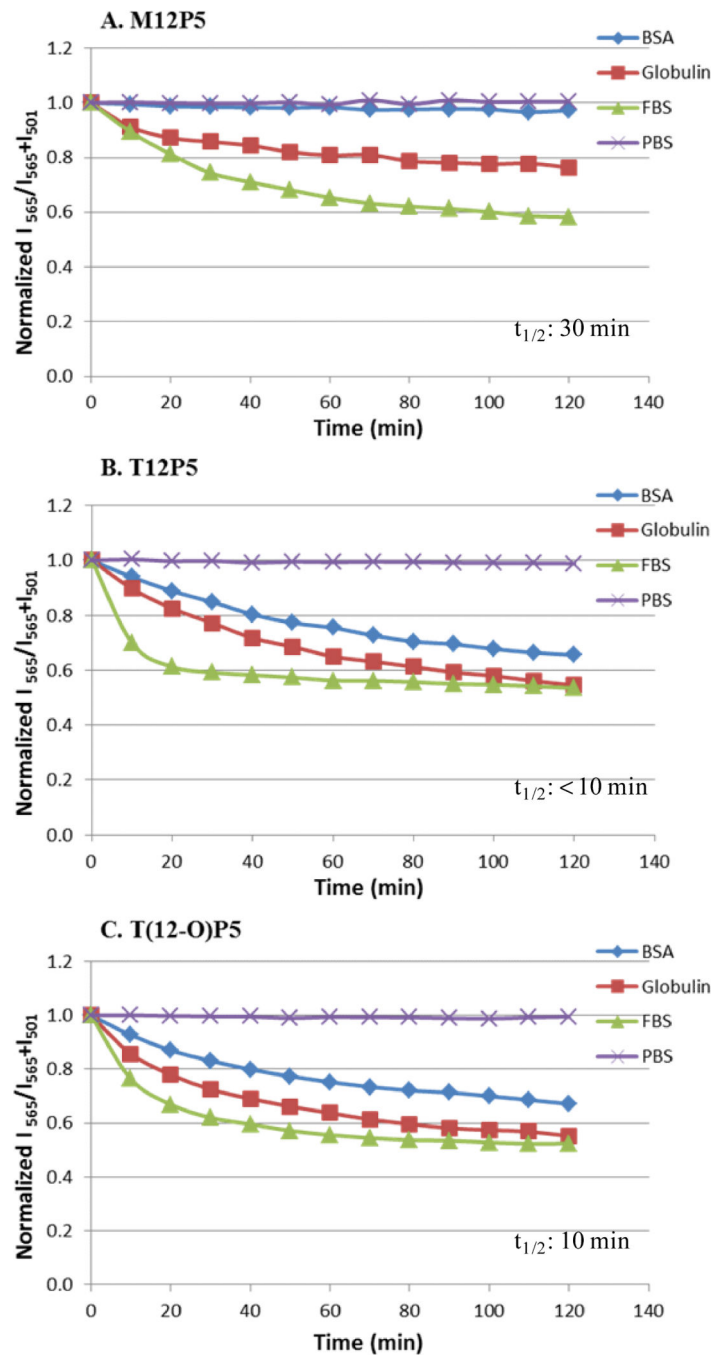
Figure 3.
Stability of FRET-loaded AMP micelles in the presence of FBS is compared to PBS (negative control), BSA, and α and β globulins. Time traces of the FRET ratio, $I_{565}/(I_{565} + I_{501})$ are normalized to time 0 in solutions. Estimated $t_{1/2}$ is indicated in dashed boxes based on each FBS curve.
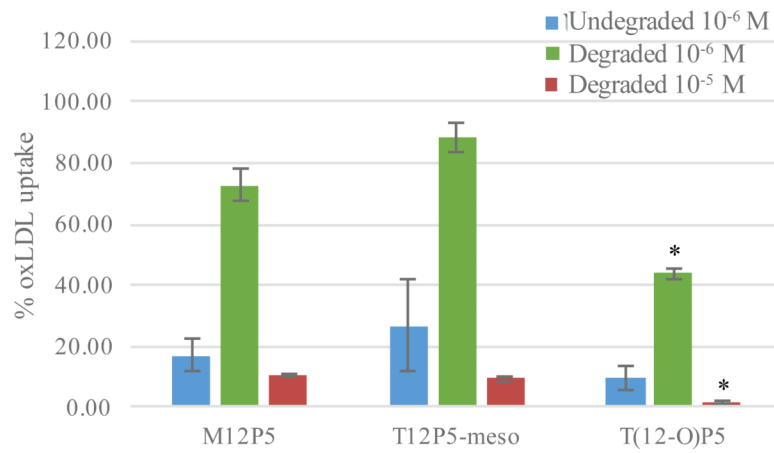
Figure 4.
OxLDL uptake of HMDMs incubated with lead AMPs pretreated with 12 U/mL lipase from porcine pancreas for 24 h in serum-free condition. Single asterisk (*) indicates statistical significance compared to M12P5 and T12P5-meso at the same concentration.
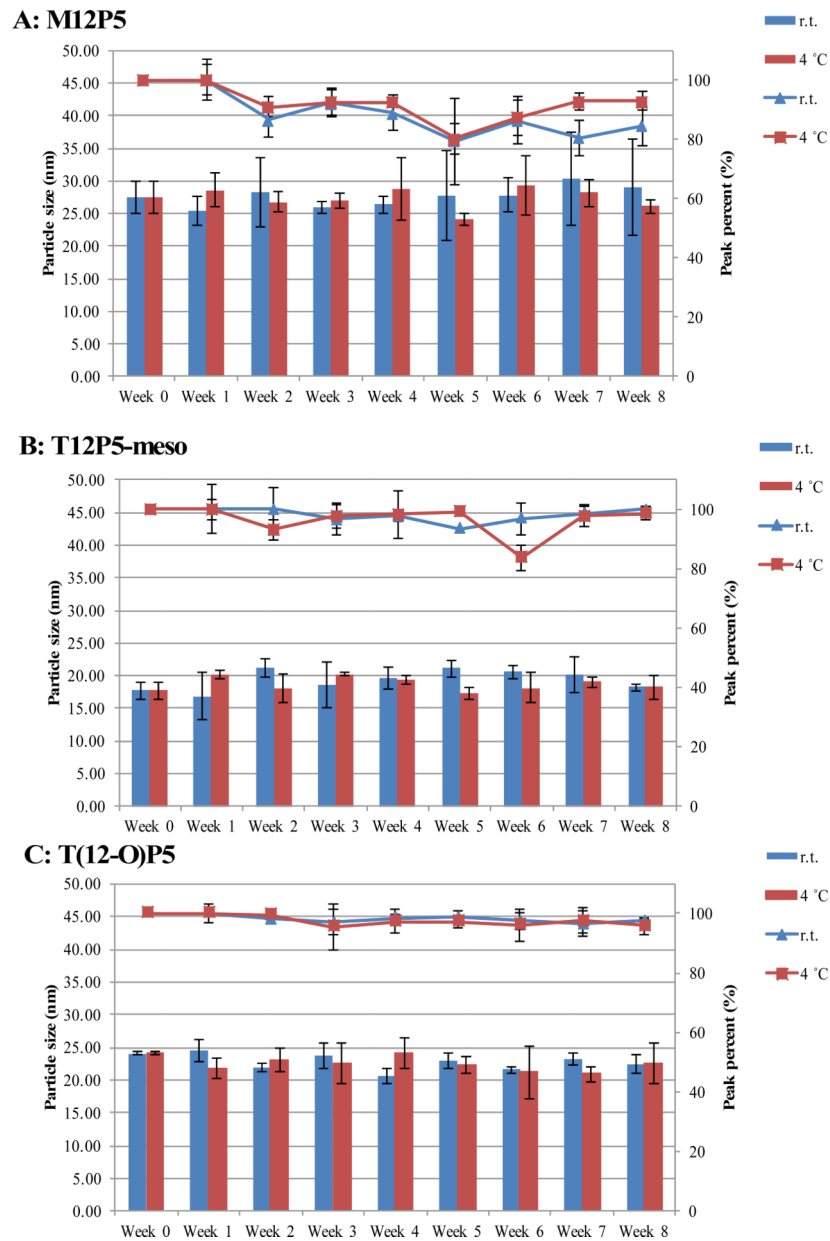
Figure 5.
Changes in particle size (bar, left y-axis) and size distribution (line, right y-axis) of AMP micelles in PBS at room temperature (blue) and 4 °C (red) over 2 months.

Table 1

Physicochemical properties of ester-linked AMPs and ether-linked AMPs as micelles at room temperature.

AMPs	Ester-linked AMPs			Ether-linked AMPs	
	M12P5	T12P5-meso	T12P5-(L)	T(12-O)P5	T(12-O)P5$_{unsat}$
Micelle size (nm)	23.7 ± 0.3	11.6 ± 1.1	15.2 ± 0.4	18.0 ± 0.2	110.0 ± 10.0
Zeta potential (mV)	−2.1 ± 0.3	−1.1 ± 0.6	−2.3 ± 0.8	−2.1 ± 0.7	−1.3 ± 0.6
CMC (mol/L)	1.2×10^{-7}	6.1×10^{-6}	6.5×10^{-5}	8.9×10^{-6}	7.0×10^{-5}

Table 2

Summary of selected AMPs' biophysical properties calculated as anionic species

AMPs/Property	Dipole (debye)	Molecular volume (Å³)	Molecular area (Å²)	Polar surface area (Å²) [%]	Non-polar surface area (Å²) [%]	< C...C>$_{avg}$ (Å)
M12P5	32	1296	1394	147 [10.5]	1247 [89.5]	5.1
T12P5-L	27.2	875	968	122 [12.6]	846 [87.4]	4.0
T12P5-meso	34.2	874	964	122 [12.7]	842 [87.3]	4.5
T(12-O)P5	23.2	742	824	97 [11.8]	727 [88.2]	4.4
T(12-O)P5$_{unsat}$	31.8	829	918	100 [10.9]	818 [89.1]	10.3